Table 1
Data collection and refinement statistics

	Crystal 1
Data collection	
Space group	$P2_12_12_1$
Cell dimensions	
a, *b*, *c* (Å)	70.4, 91.7, 152.9
α, β, γ (°)	90, 90, 90
Resolution (Å)	50–2.9 (3.0–2.9)
R_{merge}[a]	0.069 (0.212)
$I/\sigma I$	17.0 (7.0)
Completeness (%)	96.4 (79.5)
Redundancy	6.3 (5.5)
Refinement	
Resolution (Å)	44.6–2.91 (3.0–2.91)
No. reflections	21482 (1661)
R_{work}[b]/R_{free}[c]	0.218/0.273
No. atoms	
Protein	5300
Zn^{2+}	1
Ca^{2+}	5
carbohydrate	106
GM6001	28
R.m.s deviations	
Bond lengths (Å)	0.0045
Bond angles (°)	1.12

Highest resolution shell is shown in parenthesis.
[a] $R_{merge} = \sum_{hkl}\sum_i|I_i(hkl) - \langle I(hlk)\rangle|/\sum_{hkl}\sum_i I_i(hkl)$, where $I_i(hkl)$ is the *i*th intensity measurement of reflection *hkl* and $\langle I(hlk)\rangle$ is its average.
[b] $R_{work} = \sum(\| F_{obs}| - |F_{calc}\|)/\sum|F_{obs}|$.
[c] R_{free} = *R*-value for a randomly selected subset (5%) of the data that were not used for minimization of the crystallographic residual.

ing protein (IX-bp, 1J34), for the M, C and CLP domains, respectively. The final model includes amino acid residues 7-422 of the heavy chain, 1-59 and 64-133 of light chain-A (LA) and 3-123 of light chain-B (LB), and was refined to a resolution of 2.9 Å (Table 1). The overall resolution is not particularly high when compared to those of the other snake venom protein structures, most likely due to the relatively high solvent content of the crystal (~60%) and the flexible modular architecture of the MDC domains [12]. However, well-determined structural models for most sub-domains generated the electron-density maps that enable us to build a reliable model. The overall B-factor is relatively high (average B-factor of the total protein atoms is 72.2 Å^2) and the electron-densities associated with the charged side-chains located on the molecular surface (61 aa corresponding to 9% of the total model of 672 aa) are not clearly observed, however, almost all of the side-chains inside the molecule are defined in the final electron-density maps (Fig. 1B and C). Details of preparation, crystallization and structural analysis are described in the Supplementary information.

3. Results and discussion

3.1. Overall structure of RVV-X

The overall structure of RVV-X resembles a hook-spanner-wrench configuration, where the major portion of the heavy chain forms a hook and the remaining heavy chain portion and the light chains form a handle (Fig. 1A). The backbone structure of the heavy chain is essentially the same as each monomer of VAP1 [11] and catrocollastain/VAP2B [12], with the exception of the sub-domain orientations (Fig. 1D and E). There are direct, but less-specific interactions between the M and C domains, most likely resulting from crystal packing forces, such that the entire RVV-X MDC domain forms a closed C-shape structure, unlike the open C-shaped structures of VAP1 and catrocollastain/VAP2B. The M domain of RVV-X has a flat elliptical shape with a core formed by a five-stranded β-sheet and five α-helices and contains the conserved Zn^{2+}-binding HEXXHXXGXXHD sequence (residues 145–156) and a "Met-turn" (Met169) bearing the typical structural features of the metzincin family of metalloproteinases [13]. RVV-X has a fourth disulfide bridge (Cys27-Cys63) (Fig. 1B), in addition to the three conserved disulfide bridges (Cys120-Cys200, Cys160-Cys184 and Cys162-Cys167) [4] in the M domain. The M domain is followed by the D and C domains, which are further divided into shoulder (D_s), arm (D_a), wrist (C_w) and hand (C_h), segments, and the entire heavy chain folds into a C-shaped structure (Fig. 1A). The heavy chain contains three structural Ca^{2+}-binding sites and a number of disulfide bridges (9 and 5 in the D and C domains, respectively) that are highly conserved among the ADAM/adamalysin/reprolysin family proteins [11,12].

The two homologous light chains have a fold similar to the carbohydrate-recognition domain (CRD) of rat mannose binding protein (MBP) [14], but they form an intertwined dimer where the central portion of each chain projects toward the adjoining subunit (Fig. 1A). The light chains are related by a pseudo 2-fold axis which is perpendicular to the long axis of the light chain dimer.

3.2. (HVR)-mediated protein–protein interaction

RVV-X has a unique cysteine residue (Cys389) in the middle of the hyper-variable-region (HVR, residues 373–394) in C_h, a putative protein–protein interaction site for this family of proteins [11]. Cys389 forms a disulfide bond with the C-terminal cysteine residue (Cys133) of LA (Fig. 1A and C). Aside from this inter-chain disulfide bridge, Tyr346, Tyr347, and Met385 in the heavy chain form multiple hydrophobic interactions and hydrogen bonds with Tyr11, Phe12, and Pro131 in LA, which further stabilize the continuous C_h/LA structure (Fig. 1C). Most of these residues involved in the interaction between C_h and LA are not conserved among ADAMs [11,12] or among other CLPs [10]. The RVV-X structure represents the first example of HVR-mediated protein–protein interactions by the ADAM/adamalysin/reprolysin family proteins.

3.3. Light chains

Both the overall structure and the surface features of the RVV-X light chains are quite similar to those of the factor X-binding protein (X-bp) from *Deinagkistrodon actus* venom (the r.m.s. deviation of the 240 equivalent Cα atoms is 2.6 Å) determined in complex with the γ-carboxyglutamic acid (Gla) domain of factor X [15] (Fig. 2A and B). X-bp has strong anticoagulant activities because it binds to the Gla domain of factor X and inhibits its membrane-anchoring function [16]. The hydrophobic residues that are critical for the membrane-anchoring function of factor X (Phe4, Leu5 and Val8) interact with the hydrophobic patch formed by the hydrophobic residues (Met113, Ile114 and Ala115) of the B chain in X-bp [15]. Those residues are conserved in RVV-X (Phe114, Ile115 and Ala116 of LB) (Fig. 2B). The positively charged patches on X-bp that directly interact with the Gla residues in factor X are conserved, but, are less prominent in RVV-X because of amino acid substitutions (especially, Ile101 and Glu104) (Fig. 2B). The structural similarities between the RVV-X light chains and X-bp suggest the intriguing possibility that RVV-X recognizes the factor X Gla domain through an exosite, formed by the light chains (Fig. 2C).

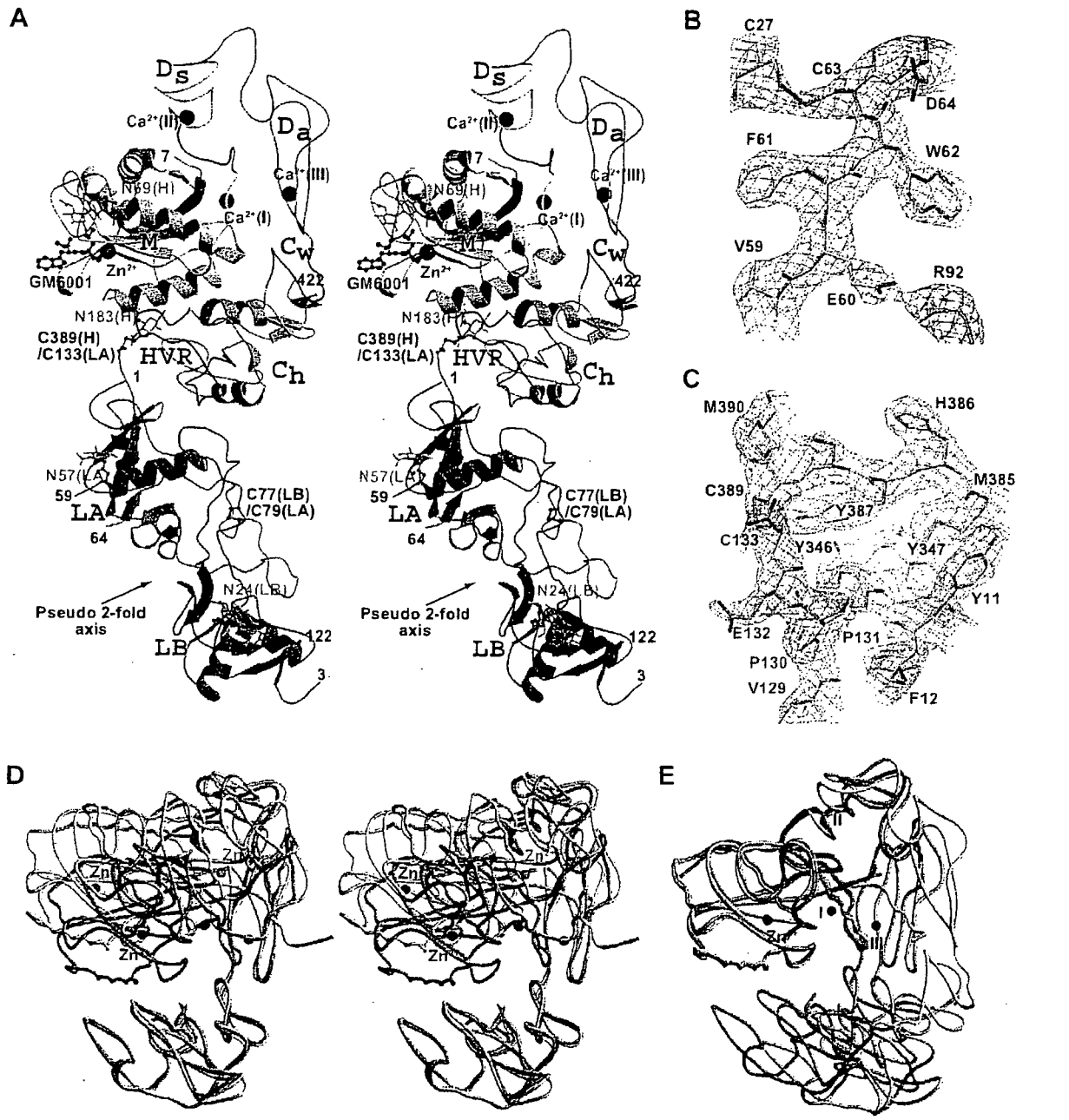

Fig. 1. Structure of RVV-X. (A) Ribbon structure of RVV-X in stereo. Bound calcium and zinc ions are represented by black and red spheres, respectively. The carbohydrate moieties (in green) linked to asparagine residues and GM6001 (in magenta) are shown in ball-and-stick representations. $2F_o - F_c$ electron-density maps (1.0σ) around the disulfide bridge between Cys27(HC) and Cys63(HC), and between Cys389 (HC) and Cys133 (LA) are represented in (B) and in (C), respectively. The HC and LA residues are labelled in black and in red, respectively. (D) Superimposition of the C_h segment of the RVV-X heavy chain (in pink) with that of the VAP1 monomer (chain-A in 2ERO, in yellow), and with that of the catrocollastatin/VAP2B (chain-A in 2DW0, in cyan) in stereo. The bound zinc and calcium atoms in RVV-X are shown as red and black spheres, respectively. The zinc atoms in VAP1 and catrocollastain/VAP2B are shown as green and blue spheres, respectively. (E) Superimposition of the M domain of the RVV-X heavy chain with the M domains of the VAP1 monomer and catrocollastatin/VAP2B.

When a properly folded Gla domain is absent from factor X, the rate of factor X activation by RVV-X is markedly diminished. In the acarboxy factor X, in which Gla formation has been blocked by a vitamin K antagonist [17] or the Des (1-44) factor X [18], factor X activation occurs at less than 1% of the rate of native factor X. Activation of factor X by RVV-X is dramatically enhanced by millimolar Ca^{2+}, which induces a conformational change in the Gla domain that enhances its binding to RVV-X [19]. Moreover, RVV-X catalyzed factor X activation is inhibited by X-bp [7]. Collectively, these observations suggest that the concave cleft created between the two light chains in RVV-X may function as an exosite for factor X-binding.

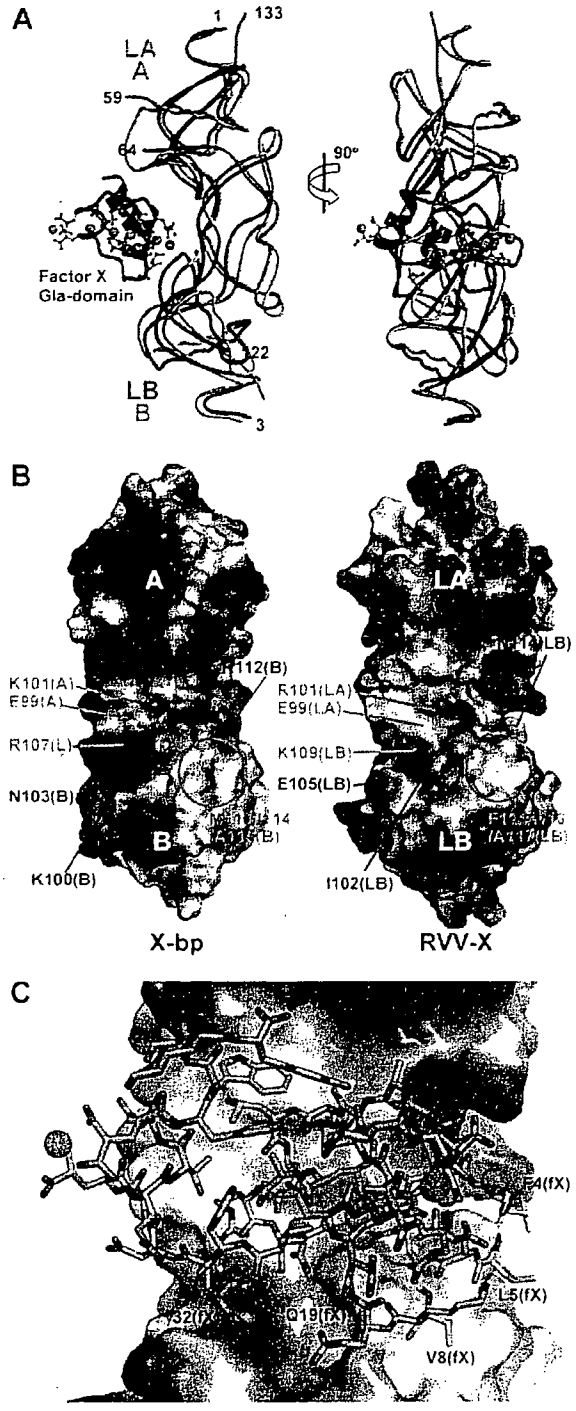

Fig. 2. Comparison of the RVV-X light chains and X-bp. (A) Superimposition of the RVV-X light chains (LA in orange and LB in magenta) onto the structure of X-bp (in gray) in complex with the Gla domain (in pink) of factor Xa (1IOD). The Gla residues and the Ca^{2+} ions are shown in ball-and-stick representation and as green spheres, respectively. (B) The molecular surfaces of X-bp and the light chains of RVV-X are represented according their electrochemical potentials (blue for positive, red for negative) and are viewed from the pseudo 2-fold axis. Conserved and varied residues are labelled in cyan and in red, respectively. (C) A model of the RVV-X light chains in complex with the Gla domain that was positioned based on the X-bp/fX Gla domain complex structure.

3.4. Docking model

Fig. 3A represents a preliminary docking model. For constructing a model, firstly, the second EGF domain (EGF2) and the serine proteinase (SP) domain of factor Xa (PDBID:1XKA) were placed such that the N-terminus of the factor X heavy chain (Ile195) closely approaches the RVV-X active site, and the globular SP domain fits into the concave

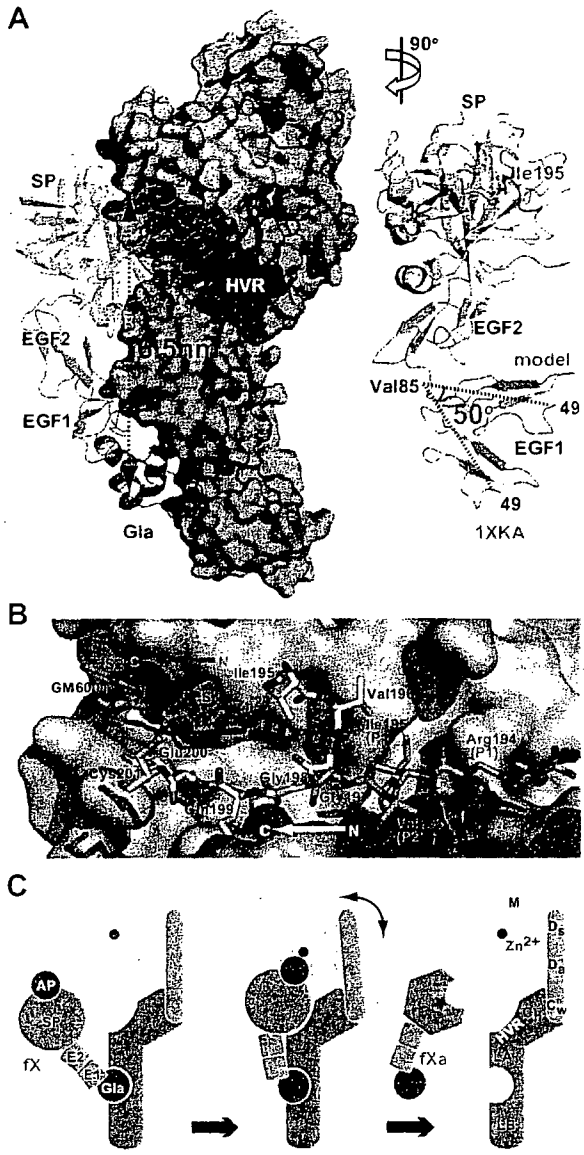

Fig. 3. Docking model. (A) The surfaces of the RVV-X sub-domains are coloured as in Fig. 1A. Factor Xa is shown in ribbon representation. Ile195 (in stick representation) and the N-terminal region (residues 195–201) of the factor X heavy chain are shown in magenta. In the right panel, the EGF1 segment of the original structural model (1XKA) is shown in gray. (B) Close up view of the RVV-X catalytic site of the docking model viewed from inside the factor Xa molecule. The N-terminal residues of factor Xa are shown in white and those of the model of factor X (zymogen) are shown in light pink. Because the factor X structure is currently unavailable, we assumed that this region has an extended structure. (C) Schematic model of factor X activation by RVV-X.

surface created by the C_h/LA domains. Secondly, we introduced a 50° bend between the two EGF domains so that the EGF1 domain fits to the convex surface of the LA domain (Fig. 3A). The linker between the two EGF domains is most likely flexible in solution [20]. This displacement successfully placed the N-terminus of the EGF1 domain in close proximity to the C-terminus of the Gla domain.

In the factor Xa structure, the N-terminal residue of the heavy chain, Ile195, is buried within the protein [20]. However, in the zymogen, the intact Arg194-Ile195-containing segment must be situated on the molecular surface, as in the equivalent segments of other serine proteinase zymogen structures [21]. The region of factor X that is C-terminal to the scissile peptide (segment coloured in magenta in Fig. 3A) may be located along the surface of the SP domain, resulting in its binding to the primed region of RVV-X, in the same orientation as the peptide-like inhibitor GM6001 lies in the current crystal structure (Fig. 3B). In the present docking model, since both molecules were positioned just as a rigid body without any collision, the active site zinc atom of RVV-X and Ile195 of factor Xa are 16 Å apart. Intrinsic hinge motions of the modular M/D_s/D_a/C_w architecture [12], and conformational changes upon association of RVV-X and the factor X zymogen, may allow the catalytic site of RVV-X to interact directly with the Arg194-Ile195 bond of factor X when in solution (Fig. 3C). The relatively large separation (~65 Å) of the catalytic site and the Gla-domain-binding exosite may explain the high specificity of RVV-X for factor X.

3.5. Implication for molecular evolution of RVV-X

CLPs from snake venoms are characterized by a unique dimerization mechanism of protein evolution, in which two monomers swap a portion of the long loop region, forming a stable functional unit and creating a new concave surface for target binding for a variety of biological activities [10]. Dimers can further aggregate with each other to form higher-order oligomers [22], or, as in the case of RVV-X, form covalently linked complexes with a metalloproteinase chain creating an exosite. The RVV-X structure illustrates a good example of evolutionary gain of function by multi-subunit proteins, represented by the fold adaptation, for the binding of other ligands.

4. Conclusion

ADAMs are widely distributed and constitute the major membrane-bound sheddases to play roles in important processes occurring at the cell surface. However, the molecular mechanism of target recognition by ADAMs and which ADAMs shed which key substrates in specific biological events has been poorly understood. Previously, we suggested that the HVR may constitute an exosite that captures the target or associated proteins, and that is processed by the catalytic site [11]. The RVV-X structure is consistent with this model and provides insights into the molecular basis of HVR-mediated protein–protein interactions and target recognition by ADAM/adamalysin/reprolysin family proteins.

Acknowledgements: The authors thank M. Tomisako for help in crystallization experiments, M. Kawamoto and N. Shimizu for assistance with data acquisition at the SPring-8 beamline BL41XU and T. Morita for helpful discussions. This work was partly supported by the Ministry of Education, Science, Sports and Culture, Grant-in-aid for Scientific Research B-19370047-2007, and Health and Labor Science Research Grants, and by grants from the Mitsubishi Pharma Research Foundation and the Astellas Foundation for Research on Metabolic Disorders. T.I is supported by the grant from New Energy and Industrial Technology Development Organization (NEDO) of Japan.

Appendix A. Supplementary data

The atomic coordinates and structure factors have been deposited in the NCBI protein data bank with the accession code 2E3X. Supplementary data associated with this article can be found, in the online version, at doi:10.1016/j.febslet.2007.11.062.

References

[1] Mann, K.G., Nesheim, M.E., Church, W.R., Haley, P. and Krishnaswamy, S. (1990) Surface-dependent reactions of the vitamin K-dependent enzyme complexes. Blood 76, 1–16.
[2] Morita, T. (1998) Proteases which activate factor X in: Enzymes from Snake Venom (Bailey, G.S., Ed.), pp. 179–208, Alaken, Colorado.
[3] Tans, G. and Rosing, J. (2001) Snake venom activators of factor X: an overview. Haemostasis 31, 225–233.
[4] Fox, J.W. and Serrano, S.M. (2005) Structural considerations of the snake venom metalloproteinases, key members of the M12 reprolysin family of metalloproteinases. Toxicon 45, 969–985.
[5] Gowda, D.C., Jackson, C.M., Hensley, P. and Davidson, E.A. (1994) Factor X-activating glycoprotein of Russell's viper venom. Polypeptide composition and characterization of the carbohydrate moieties. J. Biol. Chem. 269, 10644–10650.
[6] Kisiel, W., Hermodson, M.A. and Davie, E.W. (1976) Factor X activating enzyme from Russell's viper venom: isolation and characterization. Biochemistry 15, 4901–4906.
[7] Takeya, H., Nishida, S., Miyata, T., Kawada, S., Saisaka, Y., Morita, T. and Iwanaga, S. (1992) Coagulation factor X activating enzyme from Russell's viper venom (RVV-X). A novel metalloproteinase with disintegrin (platelet aggregation inhibitor)-like and C-type lectin-like domains. J. Biol. Chem. 267, 14109–14117.
[8] White, J.M. (2003) ADAMs: modulators of cell–cell and cell–matrix interactions. Curr. Opin. Cell Biol. 15, 598–606.
[9] Seals, D.F. and Courtneidge, S.A. (2003) The ADAMs family of metalloproteases: multidomain proteins with multiple functions. Genes Dev. 17, 7–30.
[10] Morita, T. (2005) Structures and functions of snake venom CLPs (C-type lectin-like proteins) with anticoagulant-, procoagulant-, and platelet-modulating activities. Toxicon 45, 1099–1114.
[11] Takeda, S., Igarashi, T., Mori, H. and Araki, S. (2006) Crystal structures of VAP1 reveal ADAMs' MDC domain architecture and its unique C-shaped scaffold. EMBO J. 25, 2388–2396.
[12] Igarashi, T., Araki, S., Mori, H. and Takeda, S. (2007) Crystal structures of catrocollastatin/VAP2B reveal a dynamic, modular architecture of ADAM/adamalysin/reprolysin family proteins. FEBS Lett. 581, 2416–2422.
[13] Gomis-Ruth, F.X. (2003) Structural aspects of the metzincin clan of metalloendopeptidases. Mol. Biotechnol. 24, 157–202.
[14] Weis, W.I., Kahn, R., Fourme, R., Drickamer, K. and Hendrickson, W.A. (1991) Structure of the calcium-dependent lectin domain from a rat mannose-binding protein determined by MAD phasing. Science 254, 1608–1615.
[15] Mizuno, H., Fujimoto, Z., Atoda, H. and Morita, T. (2001) Crystal structure of an anticoagulant protein in complex with the Gla domain of factor X. Proc. Natl. Acad. Sci. USA 98, 7230–7234.
[16] Atoda, H., Ishikawa, M., Mizuno, H. and Morita, T. (1998) Coagulation factor X-binding protein from Deinagkistrodon acutus venom is a Gla domain-binding protein. Biochemistry 37, 17361–17370.

[17] Lindhout, M.J., Kop-Klaassen, B.H. and Hemker, H.C. (1978) Activation of decarboxyfactor X by a protein from Russell's viper venom. Purification and partial characterization of activated decarboxyfactor X. Biochim. Biophys. Acta 533, 327–341.
[18] Morita, T. and Jackson, C.M. (1986) Preparation and properties of derivatives of bovine factor X and factor Xa from which the gamma-carboxyglutamic acid containing domain has been removed. J. Biol. Chem. 261, 4015–4023.
[19] Skogen, W.F., Bushong, D.S., Johnson, A.E. and Cox, A.C. (1983) The role of the Gla domain in the activation of bovine coagulation factor X by the snake venom protein XCP. Biochem. Biophys. Res. Commun. 111, 14–20.
[20] Kamata, K., Kawamoto, H., Honma, T., Iwama, T. and Kim, S.H. (1998) Structural basis for chemical inhibition of human blood coagulation factor Xa. Proc. Natl. Acad. Sci. USA 95, 6630–6635.
[21] Freer, S.T., Kraut, J., Robertus, J.D., Wright, H.T. and Xuong, N.H. (1970) Chymotrypsinogen: 2.5-angstrom crystal structure, comparison with alpha-chymotrypsin, and implications for zymogen activation. Biochemistry 9, 1997–2009.
[22] Fukuda, K., Mizuno, H., Atoda, H. and Morita, T. (2000) Crystal structure of flavocetin-A, a platelet glycoprotein Ib-binding protein, reveals a novel cyclic tetramer of C-type lectin-like heterodimers. Biochemistry 39, 1915–1923.

Journal of the American College of Cardiology
© 2007 by the American College of Cardiology Foundation
Published by Elsevier Inc.

Vol. 50, No. 13, 2007
ISSN 0735-1097/07/$32.00
doi:10.1016/j.jacc.2007.05.039

PRECLINICAL STUDIES

Important Role of Endogenous Hydrogen Peroxide in Pacing-Induced Metabolic Coronary Vasodilation in Dogs In Vivo

Toyotaka Yada, MD, PHD,* Hiroaki Shimokawa, MD, PHD,† Osamu Hiramatsu, PHD,* Yoshiro Shinozaki, BS,‡ Hidezo Mori, MD, PHD,§ Masami Goto, MD, PHD,* Yasuo Ogasawara, PHD,* Fumihiko Kajiya, MD, PHD*

Kurashiki, Sendai, Isehara, and Suita, Japan

Objectives We examined whether endogenous hydrogen peroxide (H_2O_2) is involved in pacing-induced metabolic vasodilation in vivo.

Background We have previously demonstrated that endothelium-derived H_2O_2 is an endothelium-derived hyperpolarizing factor in canine coronary microcirculation in vivo. However, the role of endogenous H_2O_2 in metabolic coronary vasodilation in vivo remains to be examined.

Methods Canine subepicardial small coronary arteries (≥100 μm) and arterioles (<100 μm) were continuously observed by a microscope under cyclooxygenase blockade (ibuprofen, 12.5 mg/kg intravenous [IV]) (n = 60). Experiments were performed during paired right ventricular pacing under the following 7 conditions: control, nitric oxide (NO) synthase inhibitor (N^G-monomethyl-L-arginine [L-NMMA], 2 μmol/min for 20 min intracoronary [IC]), catalase (a decomposer of H_2O_2, 40,000 U/kg IV and 240,000 U/kg/min for 10 min IC), 8-sulfophenyltheophylline (SPT) (an adenosine receptor blocker, 25 μg/kg/min for 5 min IC), L-NMMA+catalase, L-NMMA+tetraethylammonium (TEA) (K_{Ca}-channel blocker, 10 μg/kg/min for 10 min IC), and L-NMMA+catalase+8-SPT.

Results Cardiac tachypacing (60 to 120 beats/min) caused coronary vasodilation in both-sized arteries under control conditions in response to the increase in myocardial oxygen consumption. The metabolic coronary vasodilation was decreased after L-NMMA in subepicardial small arteries with an increased fluorescent H_2O_2 production compared with catalase group, whereas catalase decreased the vasodilation of arterioles with an increased fluorescent NO production compared with the L-NMMA group, and 8-SPT also decreased the vasodilation of arterioles. Furthermore, the metabolic coronary vasodilation was markedly attenuated after L-NMMA+catalase, L-NMMA+TEA, and L-NMMA+catalase+8-SPT in both-sized arteries.

Conclusions These results indicate that endogenous H_2O_2 plays an important role in pacing-induced metabolic coronary vasodilation in vivo. (J Am Coll Cardiol 2007;50:1272–8) © 2007 by the American College of Cardiology Foundation

Cardiac tachycardia by pacing or exercise increases myocardial oxygen consumption (MVO_2) and increases coronary blood flow by several mechanisms (1–3). Shear stress plays a crucial role in modulating vascular tone by endothelium-derived releasing factors (EDRFs), including nitric oxide (NO), prostacyclin (PGI_2), and endothelium-derived hyperpolarizing factor (EDHF) (4,5). Flow-induced vasodilation is mediated by either NO (6,7), PGI_2 (8), both of them (9), or EDHF (10). Matoba et al. have previously identified that endothelium-derived hydrogen peroxide (H_2O_2) is a primary EDHF in mesenteric arteries of mice and humans (11,12). Morikawa et al. (13,14) subsequently confirmed

See page 1279

From the *Department of Medical Engineering and Systems Cardiology, Kawasaki Medical School, Kurashiki, Japan; †Department of Cardiovascular Medicine, Tohoku University Graduate School of Medicine, Sendai, Japan; ‡Department of Physiology, Tokai University School of Medicine, Isehara, Japan; and the §Department of Cardiac Physiology, National Cardiovascular Center Research Institute, Suita, Japan. Dr. Yada is the winner of the Endothelium-Derived Hyperpolarizing Factor (EDHF) Tanabe Award from the Scientific Sessions of the American Heart Association, November 2005, Dallas, Texas.

This work was supported in part by grants from the Japanese Ministry of Education, Science, Sports, Culture, and Technology, Tokyo, Japan, Nos. 16209027 (to Dr. Shimokawa) and 16300164 (to Dr. Yada), the Program for Promotion of Fundamental Studies in Health Sciences of the Organization for Pharmaceutical Safety and Research of Japan (to Dr. Shimokawa), and Takeda Science Foundation 2002 (to Dr. Yada).

Manuscript received September 11, 2006; revised manuscript received April 25, 2007, accepted May 1, 2007.

that endothelial Cu,Zn-superoxide dismutase (SOD) plays an important role as an EDHF synthase in mice and humans. Miura et al. (15) demonstrated that endothelium-derived H_2O_2 is involved as an EDHF in the flow-induced vasodilation of isolated human coronary arterioles in vitro. We have recently confirmed that endogenous H_2O_2 plays an important compensatory role during coronary autoregulation (16) and reperfusion injury in vivo (17) through the interactions with NO and adenosine.

It is known that vascular α-adrenergic receptor is modulated by the endothelium in dogs (18), whereas cardiac β-adrenergic receptor is modulated by K_{Ca} channels in pigs (19) and H_2O_2 in mice (20). However, the role of endogenous H_2O_2 in metabolic coronary vasodilation in vivo remains largely unknown. In the present study, we thus examined whether H_2O_2 is involved in pacing-induced metabolic coronary vasodilation in canine coronary microcirculation in vivo.

Methods

This study conformed to the Guideline on Animal Experiments of Kawasaki Medical School and the Guide for the Care and Use of Laboratory Animals published by the U.S. National Institutes of Health.

Animal preparation. Anesthetized mongrel dogs of either gender (15 to 25 kg in body weight, n = 60) were ventilated with a ventilator (Model VS600, IDC, Pittsburgh, Pennsylvania). We continuously monitored aortic pressure and left ventricular pressure (LVP) with a catheter (SPC-784A, Millar, Houston, Texas) and blood flow of the left anterior descending coronary artery (LAD) with a transonic flow probe (T206, Transonic Systems, Ithaca, New York).

Measurements of coronary diameter by intravital microscope. We continuously monitored coronary vascular responses by an intravital microscope (VMS 1210, Nihon Kohden, Tokyo, Japan) with a needle-probe in vivo, as previously described (21). We gently placed the needle-probe on subepicardial microvessels. When a clear vascular image was obtained, end-diastolic vascular images were taken with 30 pictures/s (21).

Measurements of regional myocardial blood flow. Regional myocardial blood flow was measured by the nonradioactive microsphere (Sekisui Plastic Co. Ltd., Tokyo, Japan) technique, as previously described (22). Briefly, the microspheres suspension was injected into the left atrium 3 min after tachypacing. Myocardial flow in the LAD area was calculated according to the formula "time flow = tissue counts × (reference flow/reference counts)" and was expressed in ml/g/min (22).

Detection of H_2O_2 and NO production in coronary microvessels. 2′,7′-dichlorodihydrofluorescein diacetate (DCF) (Molecular Probes, Eugene, Oregon) and diaminorhodamine-4M AM (DAR) (Daiichi Pure Chemicals, Tokyo, Japan) were used to detect H_2O_2 and NO production in coronary microvessels, respectively, as previously described (17). Briefly, fresh and unfixed heart tissues were cut into several blocks and immediately frozen in optimal cutting temperature compound (Tissue-Tek, Sakura Fine Chemical, Tokyo, Japan). Fluorescent images of the microvessels were obtained 3 min after application of acetylcholine (ACh) by using a fluorescence microscope (OLYMPUS BX51, Tokyo, Japan) (17).

Experimental protocols. After the surgical procedure and instrumentation, at least 30 min were allowed for stabilization while monitoring hemodynamic variables. Coronary vasodilator responses were examined before and after cardiac tachypacing (60 to 120 beats/min) under the following 7 conditions with cyclooxygenase blockade (ibuprofen, 12.5 mg/kg, IV) to evaluate the role of H_2O_2 and NO without PGI_2 in a different set of animals (Fig. 1): 1) control conditions without any inhibitor; 2) L-NMMA alone (2 μmol/min intracoronary [IC] for 20 min); 3) catalase alone (40,000 U/kg intravenous [IV] and 240,000 U/kg/min IC for 10 min, an enzyme that dismutates

Abbreviations and Acronyms

CBF = coronary blood flow
DAR = diaminorhodamine-4M AM
DCF = 2′,7′-dichlorodihydrofluorescein diacetate
EDHF = endothelium-derived hyperpolarizing factor
H_2O_2 = hydrogen peroxide
L-NMMA = N^G-monomethyl-L-arginine
LAD = left anterior descending coronary artery
MVO_2 = myocardial oxygen consumption
NO = nitric oxide
PGI_2 = prostacyclin
SPT = sulfophenyltheophylline
TEA = tetraethylammonium

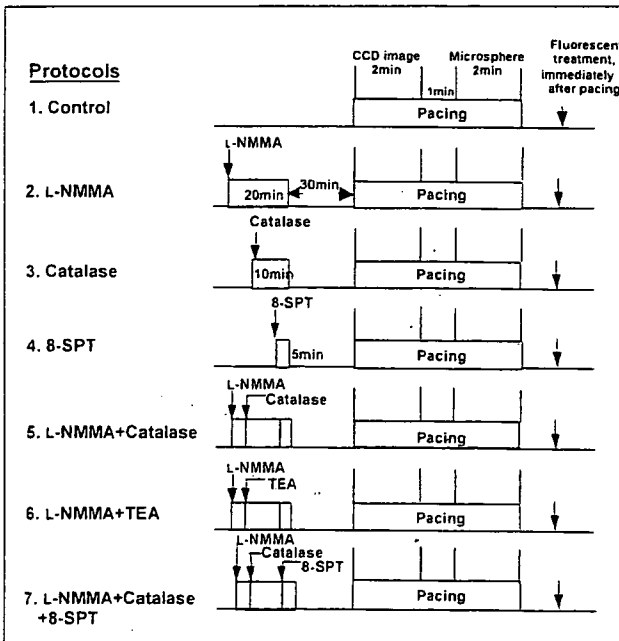

Figure 1 Experimental Protocols

CCD = charge-coupled device; L-NMMA = N^G-monomethyl-L-arginine; SPT = sulfophenyltheophylline; TEA = tetraethylammonium.

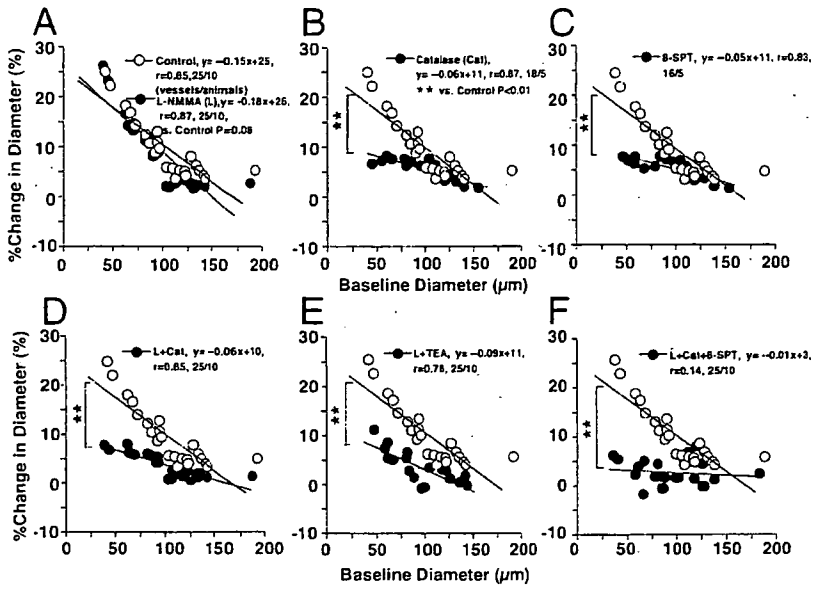

Figure 2 **Coronary Vascular Responses to Cardiac Pacing**

The coronary vasodilating responses of both-sized coronary arteries were significantly inhibited in all experimental conditions except L-NMMA alone. **p < 0.01. Abbreviations as in Figure 1.

H_2O_2 into water and oxygen); 4) adenosine receptor blockade alone (8-sulfophenyltheophylline [8-SPT], 25 μg/kg/min IC for 5 min); 5) catalase plus L-NMMA; 6) catalase plus tetraethylammonium (TEA) (10 μg/kg/min IC for 10 min, an inhibitor of large conductance K_{Ca} channels to inhibit EDHF-mediated responses) (23); and 7) catalase plus L-NMMA with 8-SPT (16). These inhibitors were given at 30 min before cardiac tachypacing (Fig. 1). The basal coronary diameter was defined as that before pacing. We continuously observed the diameter change in subepicardial small coronary arteries (≥100 μm) and arterioles (<100 μm) with an intravital microscope before and at 2 min after pacing. Microspheres were administered at 3 min after the pacing was started (Fig. 1). In the combined infusion protocol (L-NMMA+catalase+8-SPT), L-NMMA infusion was first started, followed by catalase infusion, and then 8-SPT was added at 15 min after the initiation of L-NMMA infusion (Fig. 1). Then, fresh and unfixed heart tissues were cut into several blocks and immediately frozen in optimal cutting temperature compound after the pacing. The flow and MVO_2 were measured as full-thickness values.

Drugs. All drugs were obtained from Sigma Chemical Co. and were diluted in a physiological saline immediately before use.

Statistical analysis. Results are expressed as means ± SEM. Differences in the vasodilation of subepicardial coronary microvessels before and after pacing (Fig. 2) were examined by a multiple regression analysis using a model, in which the change in coronary diameter was set as a dependent variable (y) and vascular size as an explanatory variable (x), while the statuses of control and other inhibitors were set as dummy variables (D1, D2) in the following equation: $y = a0 + a1x + a2D1 + a3D2$, where a0 through a3 are partial regression coefficients (16). Significance tests were made as simultaneous tests for slope and intercept differences. Pairwise comparisons against control were made without adjustment for multiple comparisons. The vessel was the unit of analysis without correction for correlated observations. The power of this analysis is greater than that of using the animal as the unit of analysis, giving smaller p values. Vascular fluorescent responses (Figs. 3 and 4) were analyzed by one-way analysis of variance followed by Scheffe's post hoc test for multiple comparisons. The criterion for statistical significance was at $p < 0.05$.

Results

Hemodynamic status and blood gases during pacing. Throughout the experiments, mean aortic pressure was constant and comparable (Table 1), and pO_2, pCO_2, and pH were maintained within the physiological ranges (pO_2 >70 mm Hg, pCO_2 25 to 40 mm Hg, and pH 7.35 to 7.45). Baseline coronary diameter was comparable in the absence and presence of inhibitors under the 7 different experimental conditions (Table 1). Cardiac tachypacing increased coronary blood flow and MVO_2 from the baseline values (Table 2, both $p < 0.01$). Combined infusion of L-NMMA+catalase+8-SPT significantly decreased coronary blood flow (CBF) and MVO_2 as compared with control, L-NMMA alone (both $p < 0.01$), catalase alone (both $p < 0.01$), 8-SPT alone (both $p < 0.01$), L-NMMA+catalase (both $p < 0.05$), L-NMMA+TEA (both $p < 0.05$). Com-

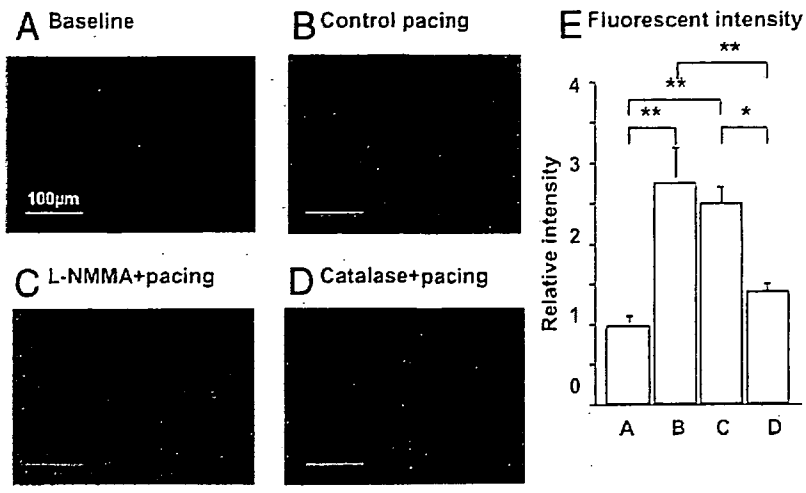

Figure 3 **Detection of H_2O_2 Production With DCF Fluorescent Method**

Hydrogen peroxide (H_2O_2) production was unaltered after N^G-monomethyl-L-arginine (L-NMMA) but was markedly suppressed by catalase. Number of arterioles/animals used was 5/5 for each group. *p < 0.05, **p < 0.01. DCF = 2′,7′-dichlorodihydrofluorescein diacetate.

bined infusion of L-NMMA+catalase or L-NMMA+TEA significantly decreased CBF (both $p < 0.05$) and MVO_2 (both $p < 0.05$) as compared with control after the pacing.

Coronary vasodilation before and after cardiac tachypacing. Cardiac tachypacing caused coronary vasodilation in both-sized arteries under control conditions (small coronary arteries, 5 ± 1%; arterioles, 14 ± 2%) (Fig. 2A) with decreased coronary venous pO_2 (Table 2). The metabolic coronary vasodilation was significantly decreased after L-NMMA in small coronary arteries (3 ± 1%) but not in arterioles (14 ± 2%), whereas catalase and 8-SPT decreased the vasodilation of arterioles (both 4 ± 1%) but not in small coronary arteries (both 7 ± 1%) (Figs. 2B and 2C). Furthermore, the metabolic coronary vasodilation was markedly attenuated after L-NMMA+catalase and L-NMMA+TEA in small coronary arteries (both 2 ± 1%), and L-NMMA+catalase+8-SPT almost abolished the vasodilating responses in both-sized arteries (small coronary arteries, −1 ± 1%; arterioles, 1 ± 1%) (Figs. 2D to 2F). When expressed in a linear regression analysis, the coronary vasodilating responses of both-sized coronary arteries were significantly inhibited in all experimental conditions except L-NMMA alone (Fig. 2A).

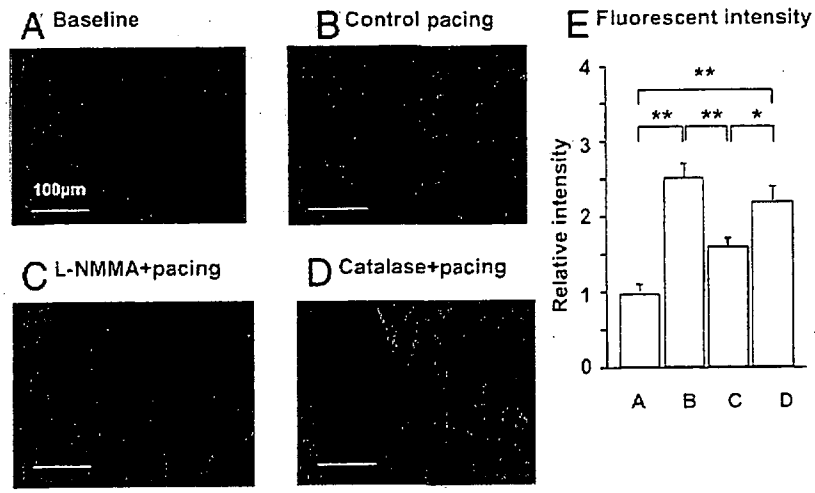

Figure 4 **Detection of NO Production With DAR Fluorescent Method**

Nitric oxide (NO) production was unaltered after catalase but was markedly suppressed by N^G-monomethyl-L-arginine (L-NMMA). Number of arterioles/animals used was 5/5 for each group. *p < 0.05, **p < 0.01. DAR = diaminorhodamine-4M AM.

JACC Vol. 50, No. 13, 2007
September 25, 2007:1272–8

Table 1 The Small Artery and Arteriolar Diameter Measurements at Rest and During Cardiac Pacing

	Control	L-NMMA (L)	Catalase (Cat)	8-SPT	L+Cat	L+TEA	L+Cat+8-SPT
Small artery							
n (vessels/dogs)	12/10	12/10	9/5	7/5	12/10	12/10	12/10
Rest (μm)	127 ± 7	125 ± 6	127 ± 5	126 ± 6	125 ± 7	123 ± 6	124 ± 7
Cardiac pacing (μm)	134 ± 7*	129 ± 7†	132 ± 5*	131 ± 6*	127 ± 7	124 ± 6	123 ± 6
Arteriole							
n (vessels/dogs)	12/10	12/10	9/5	9/5	12/10	12/10	12/10
Rest (μm)	75 ± 5	73 ± 5	71 ± 5	71 ± 5	72 ± 5	74 ± 5	72 ± 6
Cardiac pacing (μm)	85 ± 5*	82 ± 5*	77 ± 6†	77 ± 6†	77 ± 5†	77 ± 5	73 ± 5

Results are expressed as mean ± SEM. *$p < 0.01$, †$p < 0.05$ versus rest.
L-NMMA = N^G-monomethyl-L-arginine; SPT = sulfophenyltheophylline; TEA = tetraethylammonium.

Detection of H_2O_2 and NO production. Fluorescent microscopy with DCF showed that cardiac tachypacing increased coronary H_2O_2 production compared with baseline conditions in arterioles (Fig. 3). The pacing-induced H_2O_2 production as assessed by DCF fluorescent intensity was unaltered after L-NMMA but was markedly suppressed by catalase (Fig. 3). By contrast, in small coronary arteries, vascular NO production as assessed by DAR fluorescent intensity was significantly increased in response to the pacing compared with baseline conditions (Fig. 4). The pacing-induced NO production was unaltered after catalase but was markedly suppressed by L-NMMA (Fig. 4). Pacing caused no significant increase in H_2O_2 production in small coronary arteries or NO production in arterioles (data not shown).

Discussion

The major finding of the present study is that endogenous H_2O_2 plays an important role in pacing-induced metabolic coronary dilation as a compensatory mechanism for NO in vivo. We demonstrated the important role of endogenous H_2O_2 in the mechanisms for metabolic coronary dilation in vivo.

Validations of experimental model and methodology. We chose, on the basis of our previous reports (16,17), the adequate dose of L-NMMA, catalase, TEA, and 8-SPT in order to inhibit NO synthesis, H_2O_2, K_{Ca} channels, and the adenosine receptor, respectively. The TEA at low doses is fairly specific for K_{Ca} channel, but at higher doses it might block a number of other K channels. Because several K_{Ca} channels might be involved in H_2O_2-mediated responses (5), we selected nonselective K_{Ca} inhibitor, TEA, to inhibit all K_{Ca} channels (23). We have previously confirmed the validity of our present methods (21).

Role of NO and H_2O_2 after cardiac pacing. Matoba et al. have demonstrated that endothelium-derived H_2O_2 is an EDHF in mouse (11) and human (12) mesenteric arteries and pig coronary microvessels (24). Morikawa et al. also

Table 2 Hemodynamic Status at Rest and During Cardiac Pacing

	Control	L-NMMA (L)	Catalase (Cat)	8-SPT	L+Cat	L+TEA	L+Cat+8-SPT
n (dogs)	10	10	5	5	10	10	10
SBP							
Rest (mm Hg)	135 ± 14	135 ± 14	114 ± 9	123 ± 5	98 ± 9	99 ± 9	96 ± 8
Cardiac pacing	137 ± 14	136 ± 14	125 ± 12	130 ± 7	100 ± 9	100 ± 8	103 ± 9
MBP							
Rest (mm Hg)	117 ± 10	117 ± 10	98 ± 8	99 ± 5	89 ± 10	90 ± 10	87 ± 9
Cardiac pacing	124 ± 9	120 ± 13	107 ± 10	110 ± 7	91 ± 10	92 ± 10	92 ± 10
DP							
Rest	8,100 ± 845	8,100 ± 845	6,855 ± 527	7,350 ± 312	5,880 ± 537	5,910 ± 527	5,730 ± 478
Cardiac pacing	16,440 ± 1,718*	16,320 ± 1,680*	15,000 ± 1,423*	15,630 ± 778*	11,940 ± 11,029*	12,000 ± 1,011*	12,300 ± 1,078*
$CVPO_2$							
Rest (mm Hg)	20 ± 1	17 ± 1	16 ± 1	17 ± 1	15 ± 1†	15 ± 1†	14 ± 1†
Cardiac pacing	14 ± 1*	11 ± 1*	11 ± 1*	12 ± 1*	10 ± 1*†	10 ± 1*†	9 ± 1*†
MVO_2							
Rest (μlO_2/min/g)	70 ± 2	66 ± 2	67 ± 2	73 ± 5	62 ± 5	61 ± 5	60 ± 5
Cardiac pacing	171 ± 4‡	168 ± 2‡	158 ± 12‡	168 ± 13‡	133 ± 4†‡	130 ± 18†‡	95 ± 9*§
CBF							
Rest (ml/min/g)	0.66 ± 0.06	0.63 ± 0.06	0.66 ± 0.03	0.66 ± 0.01	0.59 ± 0.06	0.62 ± 0.05	0.51 ± 0.04
Cardiac pacing	1.48 ± 0.32‡	1.46 ± 0.06‡	1.36 ± 0.02‡	1.40 ± 0.01‡	1.22 ± 0.01†‡	1.24 ± 0.12†‡	0.96 ± 0.07‡§

Results are expressed as mean ± SEM. *$p < 0.05$ versus at rest. †$p < 0.05$ versus corresponding control measurements. ‡$p < 0.01$ versus rest. §$p < 0.01$ versus corresponding control measurements.
CBF = coronary blood flow; $CVPO_2$ = coronary venous pO_2; DP = double product; MBP = mean blood pressure; MVO_2 = myocardial oxygen consumption; SBP = systolic blood pressure; other abbreviations as in Table 2.

have demonstrated that endothelial Cu,Zn-SOD plays an important role as an H_2O_2/EDHF synthase in mouse (13) and human (14) mesenteric arteries. Subsequently, we (16,17) and others (15) confirmed that endogenous H_2O_2 exerts important vasodilator effects in canine coronary microcirculation in vivo and in isolated human coronary microvessels, respectively. In the present study, the pacing-induced metabolic coronary vasodilation was significantly decreased after L-NMMA in small coronary arteries but not in arterioles, whereas catalase decreased the vasodilation of arterioles but not that of small arteries, and the coronary vasodilation was markedly attenuated after L-NMMA+catalase (Fig. 2). These findings indicate that NO and H_2O_2 compensate for each other to maintain coronary vasodilation in response to increased myocardial oxygen demand. Coronary venous pO_2 tended to be lower after L-NMMA+catalase, suggesting that NO and H_2O_2 coordinately cause coronary vasodilation during cardiac tachypacing.

Saitoh et al. (25) suggested that the production of H_2O_2, which stems from the dismutation of $\cdot O_2^-$ that is formed during mitochondrial electron transport, is seminal in the coupling between oxygen metabolism and blood flow in the heart. Thus, the contribution of H_2O_2 production in response to the change in metabolism cannot be excluded.

Endothelial Cu,Zn-SOD plays an important role in the synthesis of H_2O_2 as an EDHF synthase in mouse (13) and human (14) mesenteric arteries, and exercise training enhances expression of Cu,Zn-SOD in normal pigs (26). It remains to be examined whether exercise-induced upregulation of Cu,Zn-SOD enhances metabolic coronary vasodilation mediated by endogenous H_2O_2.

Compensatory vasodilator mechanism among H_2O_2, NO, and adenosine. The EDHF acts as a partial compensatory mechanism to maintain endothelium-dependent vasodilation in the forearm microcirculation of patients with essential hypertension, where NO activity is impaired owing to oxidative stress (27). We have recently demonstrated in the fluorescent microscopy study that coronary vascular production of H_2O_2 and NO is enhanced after myocardial ischemia/reperfusion in small coronary arteries and arterioles, respectively (17). In the present study, the DCF fluorescent intensity was comparable between control and L-NMMA, and that of DAR was also comparable between control and catalase (Figs. 3 and 4). Although the exact source of vascular production of H_2O_2 and NO remains to be elucidated, it is highly possible that endothelium-derived NO and H_2O_2 compensate for each other to maintain coronary vasodilation in response to increased MVO_2.

In the dog, blockade of any vasodilator mechanisms fails to blunt the increase in coronary blood flow in response to exercise, indicating that adenosine, K^+_{ATP}-channel opening, prostanoids, or NO might not be mandatory for exercise-induced coronary vasodilation, or that these redundant vasodilator mechanisms compensate for each other when one mechanism is blocked (28). In the present study, adenosine blockade with 8-SPT alone inhibited the pacing-induced vasodilation of arteriole but not that of small artery, whereas combined administration of L-NMMA+catalase+8-SPT almost abolished the pacing-induced coronary vasodilation of both-sized arteries with an increase in coronary blood flow (Fig. 2). The discrepancy between the diameter and flow responses is likely due to the metabolic autoregulation of smaller arterioles. These results indicate that adenosine also plays an important role to maintain metabolic coronary vasodilation in cooperation with NO and H_2O_2, a finding consistent with our previous study on coronary autoregulatory mechanisms (15).

Study limitations. Several limitations should be mentioned for the present study. First, although we were able to demonstrate the production of H_2O_2 with fluorescent microscopy with DCF, we were unable to quantify the endothelial H_2O_2 production, because DCF reacts with H_2O_2, peroxynitrite, and hypochlorous acid (13). Second, we were unable to find smaller arterioles, owing to the limited spatial resolution of our charge-coupled device intravital microscope. With an intravital camera with higher resolution, we would be able to observe coronary vasodilation of smaller arterioles. Third, we were unable to determine whether H_2O_2 is produced by shear stress or cardiac metabolism. This point remains to be elucidated in a future study.

Conclusions

We were able to demonstrate that endogenous H_2O_2 plays an important role in pacing-induced metabolic coronary vasodilation in canine coronary microcirculation in vivo and that there are substantial compensatory interactions among NO, H_2O_2, and adenosine to maintain metabolic coronary vasodilation, which is one of the most important mechanisms for cardiovascular homeostasis in vivo.

Reprint requests and correspondence: Dr. Toyotaka Yada, Department of Medical Engineering and Systems Cardiology, Kawasaki Medical School, 577 Matsushima, Kurashiki, Okayama 701-0192, Japan. E-mail: yada@me.kawasaki-m.ac.jp.

REFERENCES

1. Ishibashi Y, Duncker DJ, Zhang J, Bache RJ. ATP-sensitive K^+ channels, adenosine, and nitric oxide-mediated mechanisms account for coronary vasodilation during exercise. Circ Res 1998;82:346–59.
2. Jones CJ, Kuo L, Davis MJ, DeFily DV, Chilian WM. Role of nitric oxide in the coronary microvascular responses to adenosine and increased metabolic demand. Circulation 1995;91:1807–13.
3. Yada T, Richmond KN, Van Bibber R, Kroll K, Feigl EO. Role of adenosine in local metabolic coronary vasodilation. Am J Physiol 1999;276:H1425–33.
4. Feletou M, Vanhoutte PM. Endothelium-dependent hyperpolarization of canine smooth muscle. Br J Pharmacol 1988;93:515–24.
5. Shimokawa H. Primary endothelial dysfunction: atherosclerosis. J Mol Cell Cardiol 1999;31:23–37.
6. Kuo L, Davis MJ, Chilian WM. Endothelium-dependent, flow-induced dilation of isolated coronary arterioles. Am J Physiol 1991; 259:H1063–70.

7. Kuo L, Chilian WM, Davis MJ. Interaction of pressure- and flow-induced responses in porcine coronary resistance vessels. Am J Physiol 1991;261:H1706–15.
8. Koller A, Sun D, Kaley G. Role of shear stress and endothelial prostaglandins in flow- and viscosity-induced dilation of arterioles in vitro. Circ Res 1993;72:1276–84.
9. Koller A, Sun D, Huang A, Kaley G. Corelease of nitric oxide and prostaglandins mediates flow-dependent dilation of ratgracilis muscle arterioles. Am J Physiol 1994;267:H326–32.
10. Takamura Y, Shimokawa H, Zhao H, et al. Important role of endothelium-derived hyperpolarizing factor in shear stress-induced endothelium-dependent relaxations in the rat mesenteric artery. J Cardiovasc Pharmacol 1999;34:381–7.
11. Matoba T, Shimokawa H, Nakashima M, et al. Hydrogen peroxide is an endothelium-derived hyperpolarizing factor in mice. J Clin Invest 2000;106:1521–30.
12. Matoba T, Shimokawa H, Kubota H, et al. Hydrogen peroxide is an endothelium-derived hyperpolarizing factor in human mesenteric arteries. Biochem Biophys Res Comm 2002;290:909–13.
13. Morikawa K, Shimokawa H, Matoba T, et al. Pivotal role of Cu,Zn-superoxide dismutase in endothelium-dependent hyperpolarization. J Clin Invest 2003;112:1871–9.
14. Morikawa K, Fujiki T, Matoba T, et al. Important role of superoxide dismutase in EDHF-mediated responses of human mesenteric arteries. J Cardiovasc Pharmacol 2004;44:552–6.
15. Miura H, Bosnjak JJ, Ning G, Saito T, Miura M, Gutterman DD. Role for hydrogen peroxide in flow-induced dilation of human coronary arterioles. Circ Res 2003;92:e31–40.
16. Yada T, Shimokawa H, Hiramatsu O, et al. Hydrogen peroxide, an endogenous endothelium-derived hyperpolarizing factor, plays an important role in coronary autoregulation in vivo. Circulation 2003; 107:1040–5.
17. Yada T, Shimokawa H, Hiramatsu O, et al. Cardioprotective role of endogenous hydrogen peroxide during ischemia-reperfusion injury in canine coronary microcirculation in vivo. Am J Physiol 2006;291: H1138–46.
18. Jones CJ, DeFily DV, Patterson JL, Chilian WM. Endothelium-dependent relaxation competes with alpha 1- and alpha 2-adrenergic constriction in the canine epicardial coronary microcirculation. Circulation 1993;87:1264–74.
19. Scornik FS, Codina J, Birnbaumer L, Toro L. Modulation of coronary smooth muscle K_{Ca} channels by Gs alpha independent of phosphorylation by protein kinase A. Am J Physiol 1993;265:H1460–5.
20. Tan CM, Xenoyannis S, Feldman RD. Oxidant stress enhances adenylyl cyclase activation. Circ Res 1995;77:710–7.
21. Yada T, Hiramatsu O, Kimura A, et al. In vivo observation of subendocardial microvessels of the beating porcine heart using a needle-probe videomicroscope with a CCD camera. Circ Res 1993; 72:939–46.
22. Mori H, Haruyama Y, Shinozaki H, et al. New nonradioactive microspheres and more sensitive X-ray fluorescence to measure regional blood flow. Am J Physiol 1992;263:H1946–57.
23. Masumoto A, Hirooka Y, Shimokawa H, Hironaga K, Setoguchi S, Takeshita A. Possible involvement of Rho-kinase in the pathogenesis of hypertension in humans. Hypertension 2001;38:1307–10.
24. Matoba T, Shimokawa H, Morikawa K, et al. Electron spin resonance detection of hydrogen peroxide as an endothelium-derived hyperpolarizing factor in porcine coronary microvessels. Arterioscler Thromb Vasc Biol 2003;23:1224–30.
25. Saitoh S, Zhang C, Tune JD, et al. Hydrogen peroxide: a feed-forward dilator that couples myocardial metabolism to coronary blood flow. Arterioscler Thromb Vasc Biol 2006;26:2614–21.
26. Rush JW, Laughlin MH, Woodman CR, Price EM. SOD-1 expression in pig coronary arterioles is increased by exercise training. Am J Physiol 2000;279:H2068–76.
27. Taddei S, Versari D, Cipriano A, et al. Identification of a cytochrome P450 2C9-derived endothelium- derived hyperpolarizing factor in essential hypertensive patients. J Am Coll Cardiol 2006;48:508–15.
28. Duncker DJ, Bache RJ. Regulation of coronary vasomotor tone under normal conditions and during acute myocardial hypoperfusion. Pharmacol Ther 2000;86:87–110.

Acta Physiol 2007, 191, 275–284

Characterization of ouabain-induced noradrenaline and acetylcholine release from *in situ* cardiac autonomic nerve endings

T. Yamazaki,[1] T. Akiyama,[1] H. Kitagawa,[1] F. Komaki,[1] H. Mori,[1] T. Kawada,[2] K. Sunagawa[2] and M. Sugimachi[2]

1 Department of Cardiac Physiology, National Cardiovascular Center Research Institute, Suita, Osaka, Japan

2 Department of Cardiovascular Dynamics, National Cardiovascular Center Research Institute, Suita, Osaka, Japan

Received 11 January 2007, revision requested 28 March 2007, revision received 29 May 2007, accepted 30 June 2007

Correspondence: T. Yamazaki, Department of Cardiac Physiology, National Cardiovascular Center Research Institute, 5-7-1 Fujishirodai, Suita, Osaka 565, Japan. E-mail: yamazaki@ri.ncvc.go.jp

Abstract

Aim: Although ouabain modulates autonomic nerve ending function, it is uncertain whether ouabain-induced releasing mechanism differs between *in vivo* sympathetic and parasympathetic nerve endings. Using cardiac dialysis, we examined how ouabain induces neurotransmitter release from autonomic nerve ending.

Methods: Dialysis probe was implanted in left ventricle, and dialysate noradrenaline (NA) or acetylcholine (ACh) levels in the anaesthetized cats were measured as indices of neurotransmitter release from post-ganglionic autonomic nerve endings.

Results: Locally applied ouabain (100 μM) increased in dialysate NA or ACh levels. The ouabain-induced increases in NA levels remained unaffected by cardiac sympathetic denervation and tetrodotoxin (Na^+ channel blocker, TTX), but the ouabain-induced increases in ACh levels were attenuated by TTX. The ouabain-induced increases in NA levels were suppressed by pretreatment with desipramine (NA transport blocker) and augmented by reserpine (vesicle NA transport blocker). In contrast, the ouabain-induced increases in ACh levels remained unaffected by pretreatment with hemicholinium-3 (choline transport blocker) but suppressed by vesamicol (vesicle ACh transport blocker). The ouabain-induced increases in NA levels were suppressed by pretreatment with ω-conotoxin GVIA (N-type Ca^{2+} channel blocker), verapamil (L-type Ca^{2+} channel blocker) and TMB-8 (intracellular Ca^{2+} antagonist). The ouabain-induced increases in ACh levels were suppressed by pretreatment with ω-conotoxin MVIIC (P/Q-type Ca^{2+} channel blocker), and TMB-8.

Conclusions: Ouabain-induced NA release is attributable to the mechanisms of regional exocytosis and/or carrier-mediated outward transport of NA, from stored NA vesicle and/or axoplasma, respectively, while the ouabain-induced ACh release is attributable to the mechanism of exocytosis, which is triggered by regional depolarization. At both sympathetic and parasympathetic nerve endings, the regional exocytosis is because of opening of calcium channels and intracellular calcium mobilization.

Keywords acetylcholine, Ca^{2+} channels, cat, microdialysis, Na^+,K^+-ATPase, noradrenaline.

 doi: 10.1111/j.1748-1716.2007.01749.x

It is generally accepted that ouabain modulates autonomic nerve function by inhibition of membrane Na^+,K^+-ATPase (Gillis & Quest 1979). This neuronal modulatory effect was mainly reported with *in vitro* sympathetic (Sweadner 1985), parasympathetic nerve endings (Satoh & Nakazato 1992, Gomez *et al.* 1996) and adrenal glands (Haass *et al.* 1997). Furthermore, ouabain-induced modulatory effect was reported with *in vitro* studies on motor endplate (Vyskocil & Illes 1977, Zemkova *et al.* 1990). From these *in vitro* studies, several mechanisms are presently suggested to induce release of neurotransmitter from the nerve endings. However, it is uncertain whether the manner of modulation differs between *in vivo* sympathetic and parasympathetic nerve endings. A major concern is whether ouabain induces a brisk increase in neurotransmitter efflux (spontaneous neurotransmitter release). Kranzhöfer *et al.* (1991) reported that ouabain-induced spontaneous noradrenaline (NA) release from sympathetic nerve endings. On the other hand, ouabain-induced spontaneous acetylcholine (ACh) release was reported *in vitro* studies using synaptosomes (Satoh & Nakazato 1992). No reports have described *in vivo* spontaneous ACh release evoked by ouabain. Further, a second issue is at which site ouabain induces neurotransmitter release: stored vesicle or axoplasma (Haass *et al.* 1997). NA and ACh release have been reported in stored vesicles and/or the axoplasma. It is uncertain, however, which site induces the predominant neurotransmitter release evoked by ouabain *in vivo*. Furthermore, the mechanisms underlying the neurotransmitter release evoked by ouabain remain unclear. Neuronal effects of ouabain have been attributed to the inhibitory action upon Na^+,K^+-ATPase and transmembrane sodium pump (Haass *et al.* 1997). As a consequence of the reduced sodium gradient at the plasma membrane, two possible mechanisms have been proposed to induce NA release from nerve endings; (i) carrier-mediated reversed NA transport, and (ii) Ca^{2+}-dependent exocytotic NA release. The manner and mechanisms of NA efflux have been extensively studied and accepted *in vivo* in isolated tissues (Sweadner 1985, Haass *et al.* 1997). However, it remains unclear whether these assumptions are valid in the cardiac sympathetic or parasympathetic nerve endings *in vivo*.

Cardiac dialysis technique in combination with highly sensitive measurement of NA or ACh has offered a powerful method for detecting the low level of dialysate NA or ACh obtained from the myocardial space (Akiyama *et al.* 1991, 1994). We demonstrated that dialysate NA or ACh levels were affected by local administration of pharmacological agents through dialysis probes, indicating that changes in dialysate NA or ACh levels reflect NA or ACh output from cardiac postganglionic sympathetic or parasympathetic nerve endings (Yamazaki *et al.* 1997, Kawada *et al.* 2001) respectively. Using dialysis technique, ouabain can be administered locally and it is possible to monitor NA or ACh output following locally applied ouabain (Yamazaki *et al.* 2001). Furthermore, comparison of the dialysate NA response in the presence and absence of neuronal agents can differentiate carrier-mediated NA release from calcium dependent exocytotic NA release (Yamazaki *et al.* 1997). With locally applied neuronal blockers, we examined the mechanisms and the sites underlying NA or ACh release evoked by ouabain.

Methods

Animal preparation

Adult cats were anaesthetized with pentobarbital sodium (30–35 mg kg^{-1} i.p.). The level of anaesthesia was maintained with a continuous intravenous infusion of pentobarbital sodium (1–2 mg kg^{-1} h^{-1}). The animals were intubated and ventilated with room air mixed with oxygen. Body temperature was maintained using a heated pad and lamp. All protocols were performed in accordance with the National Cardiovascular Center Research Institute Animal Care Ethics Committee guidelines that were in strict compliance with the NIH Guide for the Care and Use of Laboratory Animals. Electrocardiogram and mean arterial pressure were simultaneously monitored with a data recorder. The sixth rib on the left side was resected to expose the heart. With a fine guiding needle, one or two dialysis probes for dialysate sampling were implanted in the mid wall of the anterolateral region of the left ventricle. Heparin (100 U kg^{-1}) was administered after implantation of the dialysis probe and a maintenance dose was given every hour thereafter.

Dialysis technique

The material and properties of the dialysis probe were described previously (Akiyama *et al.* 1991, 1994). Briefly, we designed a transverse dialysis probe. Both ends of a dialysis fibre (13 mm length, 0.31 mm o.d. and 0.2 mm i.d.; PAN-1200, 50 000 molecular weight cutoff, Asahi Chemical, Tokyo, Japan) were connected and glued to polyethylene tubes (25 cm length, 0.5 mm o.d. and 0.2 mm i.d.). The dialysate NA or ACh levels were measured in separate animals. For the measurement of dialysate NA, the dialysis probe was perfused with Ringer's solution at 10 μL min^{-1}. Sampling periods were 2 min in duration (one sample volume = 20 μL), which was the minimum period necessary to collect sufficient NA for satisfactory measurement. For the measurement of dialysate ACh, Ringer's solution containing eserine (choline esterase

Journal compilation © 2007 Scandinavian Physiological Society, doi: 10.1111/j.1748-1716.2007.01749.x

inhibitor, 100 μM) was perfused at 2 μL min^{-1} and sampling periods were 15 min in duration. Dialysate sampling was started 120 min after probe implantation, when the dialysate NA or ACh concentration had reached a steady level. Each sample was collected in a microtube containing 0.1 N HCl or phosphate buffer to prevent oxidation. The dead-space volume between the dialysis and sample tube was measured. Taking this dead-space into account, samples were obtained.

Experimental protocols

In our previous study, we demonstrated that the dialysate NA or ACh levels reflect cardiac neuronal NA or ACh disposition at the nerve endings (Yamazaki *et al.* 1997, Kawada *et al.* 2001). Therefore, in the present study, we obtained dialysate samples and measured the dialysate NA or ACh levels as an index of NA or ACh output from post-ganglionic sympathetic or parasympathetic nerve endings respectively. Generally two mechanisms and sites are proposed to induce NA and ACh release from nerve endings: exocytotic (quantum) release from the stored vesicle and non-exocytotic (non-quantum) release from the axoplasma. The present studies were designed to clarify whether ouabain-induced NA or ACh efflux are affected by local administration of pharmacological agents that modify experimental conditions.

Protocol 1: Time courses of dialysate NA and ACh levels during local administration of ouabain. We examined the time course of dialysate NA and ACh levels during local administration of ouabain (100 μM). Ouabain was administered for 60 min. Dialysate NA levels were measured before and at 10-min intervals during ouabain administration. Dialysate ACh levels were collected in consecutive 15-min sampling periods.

Protocol 2: Influence of nerve transection and Na^+ channels on dialysate NA or ACh response evoked by ouabain. To test whether ouabain modulated central-mediated exocytotic neurotransmitter release, we examined the time course of ouabain-induced dialysate NA and ACh levels after transection of stellate ganglia or cervical parasympathetic nerve tract. For cardiac sympathetic denervation, the region of the stellate ganglia was exposed through the intercostal space, and bilateral transection of stellate ganglia was performed. After cardiac sympathetic denervation, heart rate response to carotid occlusion was blunted. In separate cats, cervical vagotomy was performed. We started dialysate sampling at 120 min after surgical interruption and ouabain-induced NA or ACh efflux was examined. Furthermore, to examine involvement of deporalization on NA or ACh release, ouabain-induced NA or ACh efflux was measured with addition of tetrodotoxin (TTX, 10 μM) through the dialysis probe. At 60 min after the beginning of TTX administration, we started the control sampling and examined the ouabain-induced NA or ACh response.

Protocol 3: Influence of NA-, ACh- and choline transporters on dialysate NA or ACh response evoked by ouabain. To test whether ouabain-induced neurotransmitter efflux was derived from axoplasma or stored vesicle, ouabain-induced NA or ACh efflux was examined with local administration of pharmacological agents, which affected the transport and content of neurotransmitter at the nerve endings. Membrane carrier-mediated NA transport was blocked by local administration of desipramine, whereas vesicular NA import was blocked by local administration of reserpine. In either case, ouabain-induced NA efflux was examined with the addition of desipramine (100 μM) or reserpine (10 μM) through the dialysis probe. The dosage of agent-administration was decided after referring to the previous studies (Akiyama *et al.* 1994, Yamazaki *et al.* 1997). Membrane carrier-mediated choline transport was blocked by local administration of hemicholinium-3 (10 μM), whereas vesicular ACh import was blocked by local administration of vesamicol (10 μM) (Kawada *et al.* 2001). In either case, ouabain-induced ACh efflux was examined with the addition of hemicholinium-3 or vesamicol through the dialysis probe.

Protocol 4: Influence of Ca^{2+} transporter, channel, mobilization on dialysate NA or ACh response evoked by ouabain. To test the contention that ouabain-induced neurotransmitter efflux was modulated by changes in intracellular Ca^{2+} levels, the influence of Ca^{2+} transporter, channel, mobilization on the dialysate NA or ACh response evoked by ouabain was examined. We focused on the involvement of three types of voltage-dependent Ca^{2+} channel, the L- and N types in the NA release evoked by ouabain. Sixty minutes after starting local administration of verapamil (100 μM), or ω-conotoxin GVIA (10 μM), we measured the ouabain-induced NA response. Second, we examined the involvement of plasma membrane Na^+/Ca^{2+} exchanger in the NA release evoked by ouabain. The inhibitors of membrane Na^+/Ca^{2+} exchange (dechlorobezamil; 100 μM, or KB7943; 10 μM) were locally administered through the dialysis probe and the ouabain-induced NA response was measured. Third, we examined the involvement of intracellular Ca^{2+} level in the NA release evoked by ouabain. An intracellular Ca^{2+} antagonist [3,4,5-trimethoxybenzoic acid 8-(dietyl amino)-octyl ester (TMB-8)] blocks the efflux of calcium from intracellular calcium stores without affecting influx

 doi: 10.1111/j.1748-1716.2007.01749.x

(Wiedenkeller & Sharp 1984). TMB-8 (1 mM) was locally administered through the dialysis probe and ouabain-induced NA response was measured. A similar pharmacological intervention was performed and ouabain-induced ACh responses were measured. Sixty minutes after starting local administration of verapamil (100 μM), or ω-conotoxin GVIA (10 μM), ω-conotoxin MVIIC (10 μM), we measured the ouabain-induced ACh response. The inhibitor of membrane Na^+/Ca^{2+} exchange (KB7943; 10 μM) was locally administered through the dialysis probe and the ouabain-induced ACh response was measured. Third, an intracellular Ca^{2+} antagonist (TMB-8, 1 mM) was locally administered through the dialysis probe and ouabain-induced ACh response was measured.

Analytical procedure

Dialysate NA concentrations were measured by HPLC with electrochemical detection (HPLC-ECD; Eicom, Kyoto, Japan). An alumina procedure was performed to remove the interfering compounds from the dialysate. The detection limit was 50 fmol per injection. Dialysate ACh concentration was measured directly by another HPLC-ECD. The detection limit was 50 fmol per injection. Details of HPLC-ECD for the NA and ACh measurements have been described elsewhere (Akiyama *et al.* 1991, 1994).

At the end of each experiment, the cats were killed with an overdose of pentobarbital sodium, and the implant sites were checked to confirm that the dialysis probes had been implanted within the left ventricular myocardium. Statistical analysis of the data was performed by analysis of variance (ANOVA). Statistical significance was defined as $P < 0.05$. Values are presented as mean ± SE.

Results

Protocol 1: Time course of dialysate NA and ACh levels during local administration of ouabain

Although local administration of ouabain did not affect haemodynamic parameters including heart rate, mean arterial pressure and electrocardiogram, ouabain induced the efflux of NA. Figure 1 (upper panel) shows the time course of the dialysate NA levels during local administration of ouabain (100 μM). Dialysate NA level increased significantly from 0.18 ± 0.06 nmol L^{-1} at control to 2.39 ± 0.53 nmol L^{-1} at 10, 12.92 ± 1.39 nmol L^{-1} at 20 min and 14.79 ± 1.97 nmol L^{-1} at 30 min. Subsequently, a slow decline occurred but high dialysate NA levels were maintained during locally applied ouabain. Peak level of dialysate NA ranged from 20 to 30 min after the beginning of ouabain administration. Figure 1 (lower panel) shows the time course of the dialysate ACh levels during local administration of ouabain (100 μM). Dialysate ACh level increased significantly from 0.91 ± 0.05 nmol at control to 3.6 ± 0.60 nmol L^{-1} at 0–15, 8.1 ± 1.4 nmol L^{-1} at 15–30 min and 6.8 ± 1.25 nmol L^{-1} at 30–45 min. Peak level of dialysate ACh appeared at 15–30 min after the beginning of ouabain administration.

Protocol 2: Influence of denervation and TTX on dialysate NA and ACh responses evoked by ouabain

We sampled the dialysates over 60 min of ouabain administration. To compare ouabain-induced NA or ACh levels under various interventions, ouabain-induced dialysate NA or ACh levels were subtracted from the control values. The sum of relative changes in dialysate NA or ACh (the unit: Σnmol/L) was expressed as an index of total NA or ACh release evoked by ouabain. Figure 2 (upper panel) shows the total NA release evoked by ouabain when cardiac sympathetic nerves were either intact, transected, pretreated with TTX. The ouabain-induced total NA release did not differ among them. Figure 2 (lower panel) shows the total ACh release evoked by ouabain when cardiac parasympathetic nerves were either intact, transected, or pretreated with TTX. The ouabain-induced total ACh release did not differ between the intact cardiac parasympathetic nerve and denervated groups whereas addition of TTX significantly inhibited the total ACh release by approx. 57% of vehicle.

Protocol 3: Influence of transport blocking agents on dialysate NA and ACh responses evoked by ouabain

Figure 3 (upper panel) shows the total NA release evoked by ouabain among various pharmacological interventions. Pretreatment with reserpine caused significant augmentation of the ouabain-induced total NA release whereas pretreatment with desipramine caused significant suppression of the total NA release. Figure 3 (lower panel) shows the total ACh release evoked by ouabain among various pharmacological interventions. The ouabain-induced total ACh release did not differ between the intact and hemicholinium-3 pretreated groups whereas addition of vesamicol significantly inhibited the total ACh release by approx. 45% of vehicle.

Protocol 4: Influence of Ca^{2+} mobilization on dialysate NA and ACh responses evoked by ouabain

Figure 4 (upper panel) shows the total NA release evoked by ouabain among various Ca^{2+} interventions. The total NA release in the 60 min after administration

Journal compilation © 2007 Scandinavian Physiological Society, doi: 10.1111/j.1748-1716.2007.01749.x

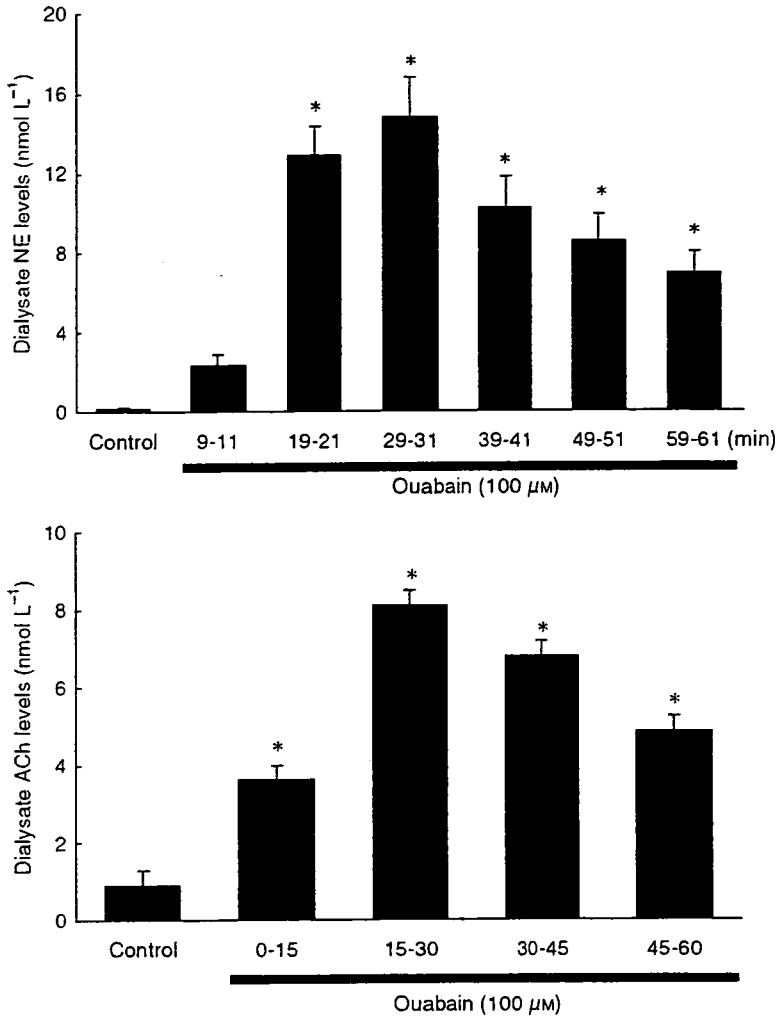

Figure 1 Upper panel: Time course of dialysate noradrenaline (NA) levels during local administration of ouabain (100 μM). Ouabain increased the dialysate NA levels. Subsequently, a slow decline occurred but high NA levels were maintained. Lower panel: Time course of dialysate acetylcholine (ACh) levels during local administration of ouabain (100 μM). Ouabain increased the dialysate ACh levels. Subsequently, a slow decline occurred but high ACh levels were maintained. Values are presented as the mean ± SE (for each column $n = 6$) $^*P < 0.05$ vs. control.

of ouabain was significantly suppressed by approx. 47% and 55% of vehicle by addition of verapamil and ω-conotoxin GVIA. Pretreatment with TMB-8 caused significant suppression of the ouabain-induced total NA release whereas pretreatment with neither KB-7943 nor dechlorobezamil altered the total NA release. Figure 4 (lower panel) shows the total ACh release evoked by ouabain among various Ca^{2+} interventions. The total ACh release in the 60 min after administration of ouabain was significantly suppressed by approx. 57% of vehicle by addition of ω-conotoxin MVIIC. Pretreatment with neither verapamil nor ω-conotoxin GVIA altered the total ACh release. Pretreatment with TMB-8 caused significant suppression of the ouabain-induced total ACh release whereas pretreatment with KB-7943 did not alter the total ACh release.

Discussion

The present study indicates that in an *in vivo* preparation, ouabain alone induced NA or ACh release from sympathetic or parasympathetic nerve endings respectively. This discussion addresses mainly similarities and differences in ouabain alone induced NA or ACh releasing sites and mechanisms.

Regional depolarization evoked by ouabain

At the post-ganglionic nervous endings, ouabain induced NA and ACh release. The transection of sympathetic or parasympathetic nerve did not affect the amount of NA or ACh release evoked by ouabain. After the transection of cardiac sympathetic or parasympathetic nerves, ouabain at 100 μM induced increases in dialysate NA or ACh levels, which were as much as those evoked by electrical stimulation of the autonomic nerve (Akiyama *et al.* 1994, Yamazaki *et al.* 1997). These data suggest that ouabain itself induces regional depolarization following exocytosis. In the case of locally administered ouabain, ouabain produced intracellular Na^+ accumulation evoked by the inhibition of Na^+,K^+-ATPase (McIvor & Cummings 1987).

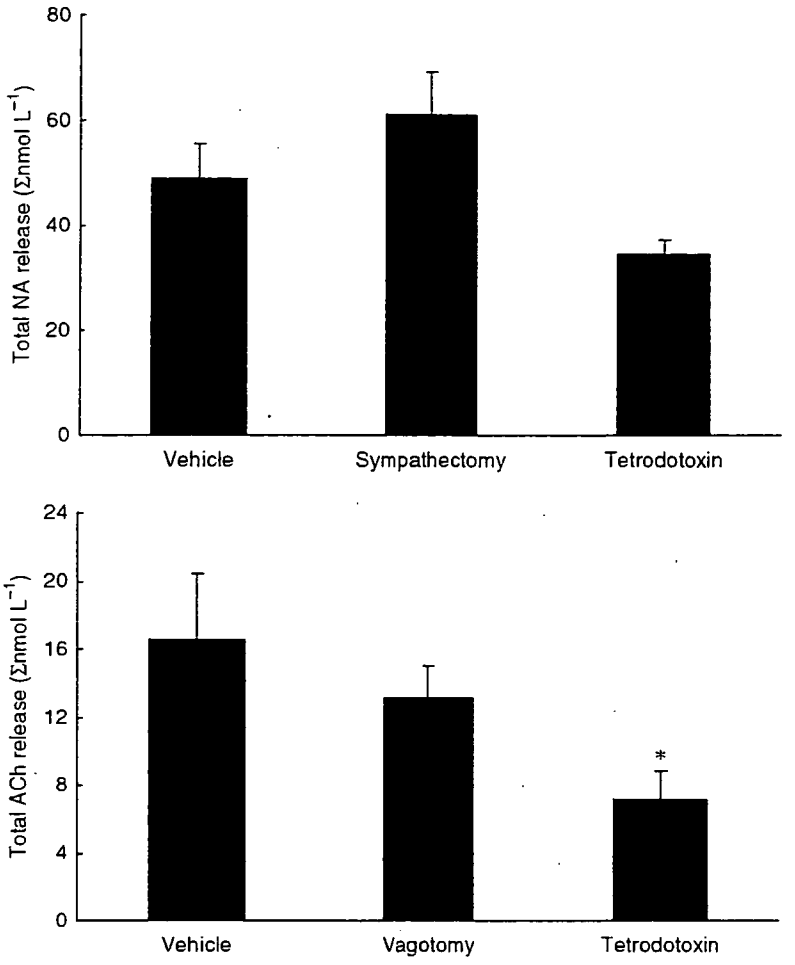

Figure 2 Upper panel: Ouabain-induced dialysate noradrenaline (NA) release in vehicle, cardiac sympathetic denervated and tetrodotoxin pretreated groups. Total NA release evoked by ouabain did not differ among the three groups. Lower panel: Ouabain-induced dialysate acetylcholine (ACh) release in vehicle, cardiac vagal denervated and tetrodotoxin pretreated groups. Total ACh release evoked by ouabain was suppressed by the pretreatment with tetrodotoxin. Values are presented as the mean ± SE (for each column $n = 6$). $^*P < 0.05$ vs. vehicle.

Regional depolarization may occur because of intracellular Na^+ accumulation (Calabresi *et al.* 1999, Dierkes *et al.* 2006). Similar finding was observed on motor endplate (Zemkova *et al.* 1990). Ouabain can increase the spontaneous ACh release by progressive decline in membrane potential when Na^+ pump is inhibited. If regional depolarization does indeed induce ACh or NA release via exocytosis from the stored vesicle, then pretreatment with TTX could inhibit this response. Local administration of TTX markedly inhibits ACh release whereas it only slightly inhibits the NA release evoked by ouabain. These results indicate that ouabain caused regional depolarization and exocytotic ACh release at the parasympathetic nerve endings. This conclusion is consistent with *in vitro* studies reported by Satoh & Nakazato (1992), and raises the question as to why TTX inhibited the ACh release but not the NA release evoked by ouabain. In the case of NA efflux evoked by ouabain, intracellular Na^+ accumulation may lead to a reduction in the Na^+ gradient between the intracellular and extracellular spaces. This reduced Na^+ gradient may cause carrier-mediated outward NA transport from axoplasma (Sharma *et al.* 1980). The threshold for intracellular Na^+ accumulation coupled to carrier-mediated outward NA transport might be lower than that for regional depolarization. Thus Na^+ accumulation coupled to regional depolarization may occur at the parasympathetic nerve endings but not at the sympathetic nerve endings.

The sites of neurotransmitter efflux evoked by ouabain

In general, two possible sites (the stored vesicle and axoplasma) were proposed to derive efflux of neurotransmitter at the nerve endings (Smith 1992, Vizi 1998). In the cholinergic nerve endings, a quantum amount of ACh was released from the stored vesicle via depolarization. Furthermore, a non-quantum amount of ACh seems to be leaked from the axoplasma without ACh transporter (Nikolsky *et al.* 1991). Local administration of vesamicol suppressed the ACh efflux evoked by ouabain. In contrast, local administration of hemicholinium-3 did not affect the ACh efflux evoked by ouabain. These data suggested that the ACh efflux was predominantly derived from the stored vesicle. This finding is consistent with the above-mentioned

Journal compilation © 2007 Scandinavian Physiological Society, doi: 10.1111/j.1748-1716.2007.01749.x

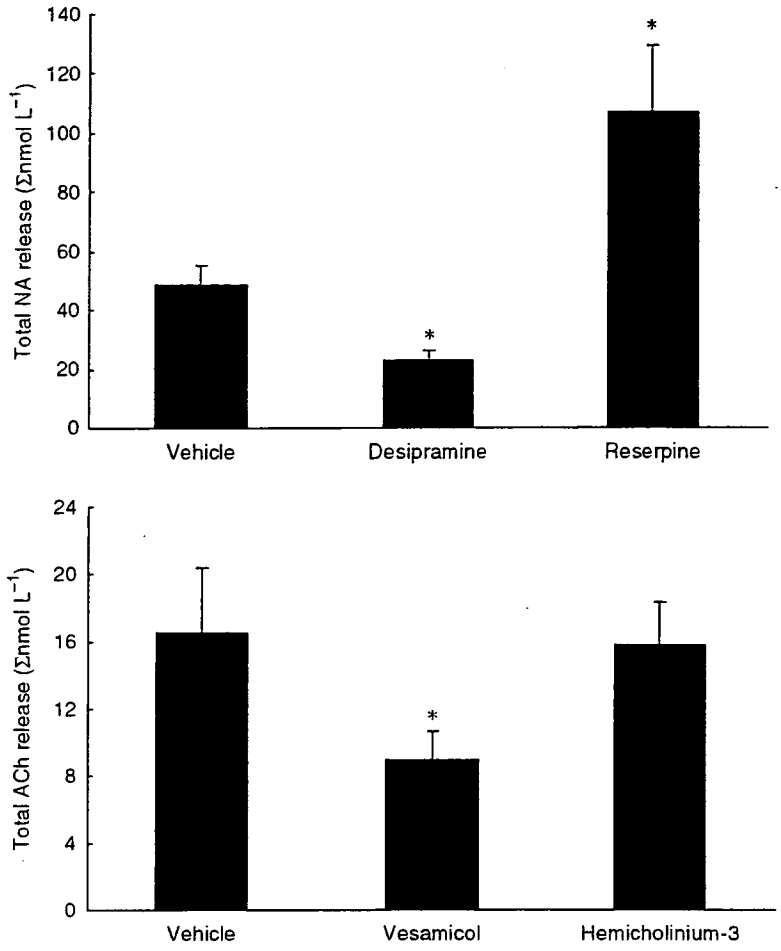

Figure 3 Upper panel: Ouabain-induced dialysate noradrenaline (NA) release among vehicle, desipramine and reserpine pretreated groups. Total NA release evoked by ouabain was suppressed by the pretreatment with desipramine and augmented by that with reserpine. Lower panel: Ouabain-induced dialysate acetylcholine (ACh) release in vehicle, vesamicol and hemicholinium-3 pretreated groups. Total ACh release evoked by ouabain was suppressed by the pretreatment with vesamicol. Values are presented as the mean ± SE (for each column $n = 6$). $^*P < 0.05$ vs. vehicle.

mechanism. Our data did not rule out the possibility of ACh efflux from the axoplasma. Vesamicol lowered the non-quantum ACh release by blocking the incorporated vesicle transporter in the terminal membrane (Edward *et al.* 1985). This involvement seems to be smaller than the involvement of ACh efflux from the stored vesicle.

Previous studies suggested that two different mechanisms (exocytosis and carrier-mediated outward transport) contributed to the amount of NA efflux evoked by ouabain (Kranzhöfer *et al.* 1991, Haass *et al.* 1997). The exocytotic NA release derived from the stored vesicle, whereas NA transporter carried out NA from the axoplasmic site via a reduced Na^+ gradient. However, it is uncertain which mechanism is predominantly involved in ouabain-induced NA efflux. To examine which site predominantly induced the neurotransmitter efflux evoked by ouabain, we administered vesicle and membranous amine transport blockers, which affected the neurotransmitter efflux evoked by ouabain. If NA efflux predominantly derives from the axoplasmic site, reserpine could increase axoplasmic NA level and augment the outward NA transport evoked by ouabain. Furthermore, as desipramine impairs carrier-mediated NA transport in both directions, desipramine could block NA efflux. NA release evoked by ouabain was augmented by local administration of reserpine but suppressed by desipramine. These data support the contention that ouabain-induced NA efflux is predominantly derived from the axoplasmic site.

Involvement of Ca^{2+} on ouabain-induced neurotransmitter efflux

Most *in vitro* studies suggested that ouabain somehow increases intracellular Ca^{2+} levels at the nerve endings and synaptosomes (Katsuragi *et al.* 1994, Casali *et al.* 1995, Wasserstrom & Aistrup 2005). Ouabain-induced intracellular Na^+ accumulation could evoke an elevation of intracellular Ca^{2+} level via Ca^{2+} channel opening (Katsuragi *et al.* 1994), Ca^{2+} release from internal stores (Nishio *et al.* 2004), and/or Na^+/Ca^{2+} exchange (Verbny *et al.* 2002). Thus, the elevation of intracellular Ca^{2+} may be associated with NA or ACh release from the autonomic nerve endings. At the parasympathetic nerve endings, neither verapamil nor ω-conotoxin GVIA

 doi: 10.1111/j.1748-1716.2007.01749.x

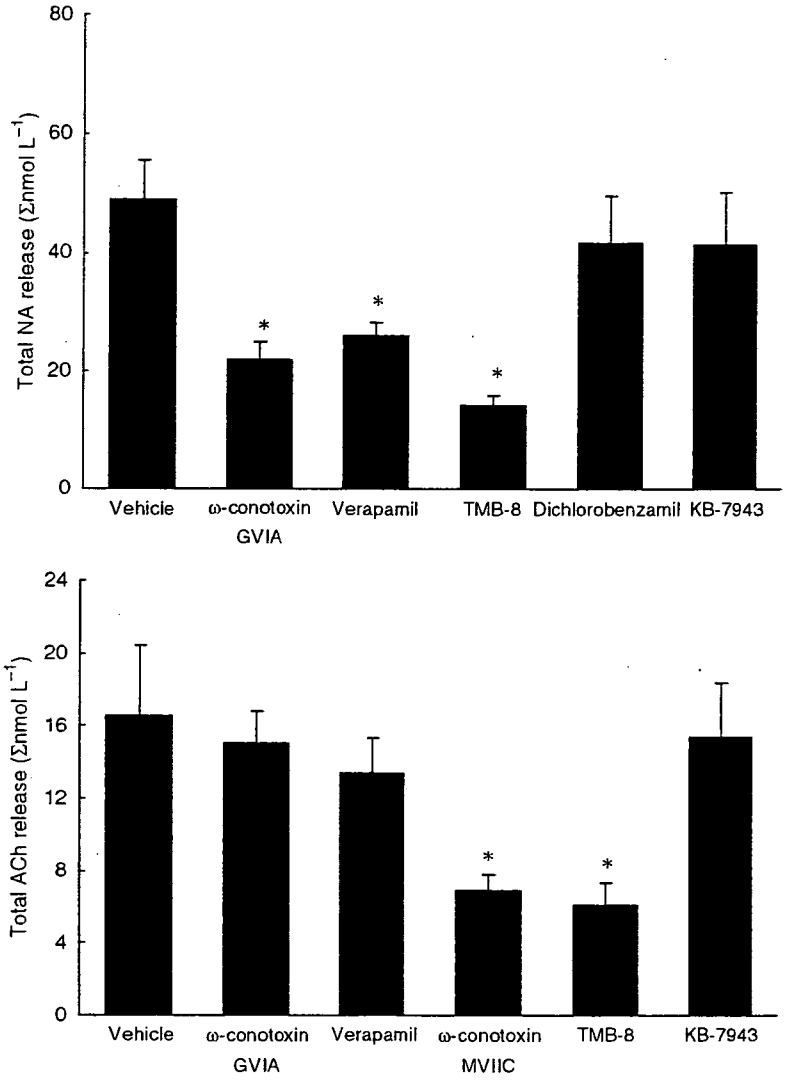

Figure 4 Upper panel: Ouabain-induced dialysate noradrenaline (NA) release in various Ca^{2+} interventions. Total NA release evoked by ouabain was suppressed by the pretreatment with ω-conotoxin GVIA, verapamil, TMB-8. Lower panel: Ouabain-induced dialysate acetylcholine (ACh) release in various Ca^{2+} interventions. Total ACh release evoked by ouabain was suppressed by the pretreatment with ω-conotoxin MVIICA or TMB-8. Values are presented as the mean ± SE (for each column $n = 6$). $^*P < 0.05$ vs. vehicle.

affected ACh release but ω-conotoxin MVIIC inhibited ACh release evoked by ouabain. Furthermore, KB-7943 did not affect either the ACh release evoked by ouabain. These data suggest that N or L-type Ca^{2+} channels or reversal Na^+/Ca^{2+} exchange might not be responsible for the ACh release evoked by ouabain. However, a marked suppression of ouabain-induced ACh release was observed with the addition of P/Q types channel blocker or TMB-8. In the case of parasympathetic nerve endings, Ca^{2+} elevation coupled to ACh release might be derived via internal stores or Ca^{2+} channels (P/Q types) rather than Na^+/Ca^{2+} exchange (Casali *et al.* 1995, Kawada *et al.* (in press)).

In the case of NA, ω-conotoxin GVIA or verapamil suppressed the NA release evoked by ouabain. Ouabain-induced NA release was independent of depolarization (TTX-resistant) but associated with the opening of Ca^{2+} channel. Furthermore, neither KB-7493 nor dichlorobenzamil affected the NA release evoked by ouabain. These data suggest that bi-directions of Na^+/Ca^{2+} exchange might not be responsible for the elevation of intracellular Ca^{2+} levels evoked by ouabain. A marked suppression of ouabain-induced NA release was observed with the addition of TMB-8. Taking these findings together, in the case of sympathetic nerve endings, Ca^{2+} elevation coupled to NA release might be derived via Ca^{2+} channels or internal store rather than membrane Na/Ca^{2+} exchange.

Although the type of Ca^{2+} channel for the NA or ACh release differed, involvement of cytosol Ca^{2+} in ouabain-induced neurotransmitter release did not differ between the parasympathetic and sympathetic nerve endings. However, the relation between TTX sensitive Na^+ channel and Ca^{2+} channel opening may differ between the parasympathetic and sympathetic nerve endings. In the present study, ouabain-induced NA efflux was suppressed by ω-conotoxin GVIA but not by TTX, indicating that TTX sensitive depolarization was not involved in Ca^{2+} channel opening coupled to exocytotic NA release. In contrast to NA release,

Journal compilation © 2007 Scandinavian Physiological Society, doi: 10.1111/j.1748-1716.2007.01749.x